PHYSICAL REVIEW B **91**, 195441 (2015)

Barrier-free subsurface incorporation of 3*d* metal atoms into Bi(111) films

C. Klein,[1,*] N. J. Vollmers,[2] U. Gerstmann,[2,†] P. Zahl,[3] D. Lükermann,[4] G. Jnawali,[1,‡] H. Pfnür,[4] C. Tegenkamp,[4] P. Sutter,[3] W. G. Schmidt,[2] and M. Horn-von Hoegen[1]

[1]*Fakultät für Physik und Center for Nanointegration (CENIDE), Universität Duisburg-Essen, Lotharstrasse 1, 47057 Duisburg, Germany*
[2]*Lehrstuhl für Theoretische Physik, Universität Paderborn, 33098 Paderborn, Germany*
[3]*Center for Functional Nanomaterials, Brookhaven National Laboratory, Upton, New York 11973, USA*
[4]*Institut für Festkörperphysik, Leibniz Universität Hannover, Appelstrasse 2, Hannover, Germany*

(Received 11 December 2014; revised manuscript received 1 May 2015; published 27 May 2015)

By combining scanning tunneling microscopy with density functional theory it is shown that the Bi(111) surface provides a well-defined incorporation site in the first bilayer that traps highly coordinating atoms such as transition metals (TMs) or noble metals. All deposited atoms assume exactly the same specific sevenfold coordinated subsurface interstitial site while the surface topography remains nearly unchanged. Notably, 3*d* TMs show a *barrier-free* incorporation. The observed surface modification by barrier-free subsorption helps to suppress aggregation in clusters. It allows a tuning of the electronic properties not only for the pure Bi(111) surface, but may also be observed for topological insulators formed by substrate-stabilized Bi bilayers.

DOI: 10.1103/PhysRevB.91.195441 PACS number(s): 68.43.Fg, 68.37.Ef, 68.43.Bc, 73.20.−r

I. INTRODUCTION

Materials with spin-polarized two-dimensional (2D) surface states arising from the Rashba effect and topological insulators are of large potential interest for spintronic or dissipationless devices. Among the special properties of such systems are the suppression of backscattering, the existence of spin-polarized currents, and the topological protection of the surface state. Besides bismuth chalcogenides such as Bi_2Se_3 and Bi_2Te_3, also Bi bulk is a well-known model system for materials with strongly spin-split surface states [1–6]. Application of these novel material systems, however, requires the controlled tuning of properties such as band gap, carrier density, or doping level by electronic or morphological manipulation [7–11]. Often the electron transport in 2D surface electron systems is strongly influenced by individual scatterers, e.g., single atoms or molecules [7,8,12]. Unintentional defects such as step edges or impurities frequently show pronounced scattering patterns in scanning tunneling microscopy (STM) [7,13–19]. In contrast to these uncontrolled surface modifications, the deposition of single atoms at the surface, usually followed by thermally activated in-diffusion, allows for intentional doping of the near-surface region. Such controlled modification was recently reported for Bi_2Se_3 and Bi_2Te_3 compound films [18,20,21]. Depending on deposition temperature and subsequent annealing, Fe atoms occupy, however, various different metastable interstitial or substitutional sites [20].

In this work, we apply a similar approach to high-quality (111) bismuth films and demonstrate the incorporation of individual impurity atoms into highly specific, well-defined subsurface interstitial sites: Combining STM and density functional theory (DFT), we show that the first Bi bilayer traps transition metal (TM) or noble metal atoms in exactly the same highly coordinated interstitial site. Moreover, 3*d* TMs such as Fe, Co, and Ni show a barrier-free incorporation. No thermal activation is required. Even at temperature below 10 K, the deposited atoms occupy always the same sevenfold coordinated subsurface site. The neighboring Bi atoms relax towards the interstitial impurity atom, but do not protrude and, thus, the surface remains structurally almost unchanged. This contrasts with typical adsorption, surface alloying, or surface reconstruction phenomena. In the following, we will refer to this special kind of surface modification as *subsorption.* It allows for the preparation of nominally undoped systems with metallic and even ferromagnetic electronic states, where backscattering is still suppressed by Rashba splitting. The barrier-free subsorption is not restricted to pure Bi(111) surfaces, but may also be found in the case of Bi(111) bilayer islands and substrate-stabilized Bi bilayers [19,22–26].

II. EXPERIMENTAL DETAILS

Ultrastable low-temperature scanning tunneling microscopy (LT-STM) was used to image and identify Friedel-like electronic scattering patterns as fingerprints for foreign atoms in a subsorption site. All experiments were performed under ultrahigh-vacuum (UHV) conditions. The preparation chamber had a base pressure below 2×10^{-10} mbar. The measurements were performed using a LT-STM in a bath cryostat at a pressure below the detection limit of 10^{-13} mbar and a base temperature of 5 K. Virtual Bi(111) substrates were grown on Si samples cut from an As-doped Si(111) wafer with a miscut below 0.1° and a resistivity of 0.004 Ω cm at room temperature. All samples were degassed in the load lock for 12 h at a temperature of 600 °C prior to transfer into UHV. A short flash annealing cycle up to 1200 °C was performed to remove the native oxide resulting in a clear (7×7) reconstruction on Si(111). Afterwards Bi was deposited by evaporation from a ceramic crucible heated by a tantalum filament. Bi(111) films were prepared by deposition of 20 nm of Bi at a sample temperature of 80 K, followed by an additional annealing step for 30 min at 200 °C [27]. This preparation results in an atomically smooth surface with

*claudius.klein@uni-due.de
†uwe.gerstmann@uni-paderborn.de
‡Present adress: Department of Physics and Astronomy, University of Pittsburgh, Pittsburgh 15260, USA.

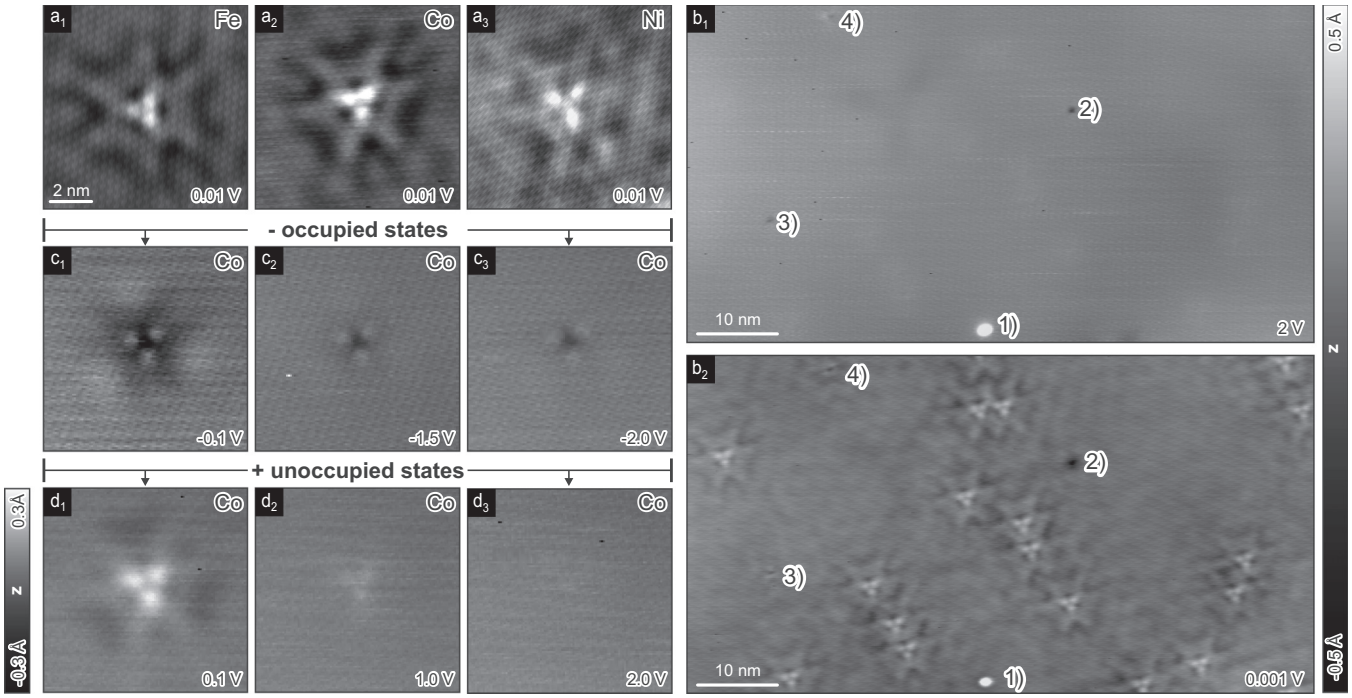

FIG. 1. (a_1–a_3) examples of various impurity atoms: Fe, Co, and Ni. (b_1) and (b_2) show a STM image of single Co impurities on a 20 nm Bi(111) film in constant current mode and identical z scale (–0.5 to 0.5 Å), taken under different conditions: (b_1) $I = 0.05$ nA, $U_{\text{Bias}} = 2$ V, and (b_2) $I = 0.05$ nA, $U_{\text{Bias}} = 1$ mV. The markers 1) to 4) indicate few other impurities or defects of unknown origin. (c_1–c_3) and (d_1–d_3): Series of a single Co impurity for various U_{Bias} ranging from -2 to $+2$ V. The z scale (-0.3 to 0.3 Å) is identical in all the images (a), (c), and (d).

terrace widths of more than 100 nm. The film quality was verified *in-situ* by low-energy electron diffraction (LEED) and STM. The low-temperature electron transport in such Bi films is dominated by a high density of surface-state electrons of about $10^{13}/\text{cm}^2$ and a negligible carrier concentration in the film bulk [28,29]. Submonolayer (ML) amounts of single-atom metal impurities were deposited onto the bare Bi films at 5 K into the STM without detaching the sample. Thereby we used a home-built microevaporator mounted on a transferable sample plate. During deposition the sample temperature increased by less than $\Delta T = 10$ K, due to radiation of the evaporator filament. The Bi(111) bilayer step height of 3.94 Å was used as calibration for the z piezo. Figures 1(a_1)-1(a_3) show STM micrographs in constant current mode after deposition of about 0.005 ML of the transition metal impurities Fe, Co, and Ni at a base temperature of 5 K (1 ML corresponds to 1 atomic layer of the Bi(111) surface, i.e., 1 ML $= 5.6 \times 10^{14}$ atoms/cm^2). Each impurity is surrounded by a threefold pattern of an apparent height modulation of $\Delta z = +0.3$ Å to -0.1 Å.

We choose the example of Co to investigate the nature and origin of the threefold patterns in more detail. Surprisingly, no signs of the deposited TM atoms are visible in Fig. 1(b1), which shows an overview STM image obtained at a bias voltage of $U = +2.0$ V. Only a few unidentified impurities or defects (labeled 1–4 in Fig. 1) are present. They do not show any scattering pattern, but can still be identified at tunneling conditions close to the Fermi level $U_{\text{Bias}} \cong 0$ V [see Fig. 1(b2). At this bias voltage, additional extended patterns with threefold symmetry become apparent, which were not observed prior to Co deposition. All of these threefold patterns have the same orientation, shape, apparent vertical amplitude, and lateral size. The density of these highly specific patterns scales with the Co deposition time, suggesting that the patterns coincide with the location of the Co atoms. Each pattern is thus indicative for the presence of a single Co atom located at the center of the pattern in the same geometrical site on or within the Bi film, interacting with (i.e., scattering) 2D electrons in the Bi(111) surface state.

Figures 1(c_1)–1(c_3) and 1(d_1)–1(d_3) show a single Co impurity for different bias voltages in higher resolution. Dominated by three light spots with trigonal symmetry, the pattern can be observed for positive and negative bias voltages, i.e., for occupied and empty states, close to the Fermi energy. The contrast and shape of the pattern, however, change significantly when varying the tunneling conditions in this regime. Some of the outer features in the threefold pattern even undergo a contrast inversion. The dispersion of the pattern, the weak amplitude at negative bias, and in particular the apparent absence of morphological features for higher bias voltages above 1 eV [see Fig. 1(d_3)] exclude a geometric height undulation as its origin. In contrast to Refs. [7,8], where morphological features such as Bi adatoms or clusters cause comparable scattering patterns, we do not observe any feature in the center of the Co-induced pattern. The pattern resembles, however, those in Bi_2Te_3(111) films where Fe atoms occupy substitutional Bi sites [20].

III. COMPUTATIONAL METHOD

The experimental observations strongly evidence that even without thermal activation all Co atoms are incorporated into the Bi film at identical subsurface sites without any morpho-

logical modification at the surface. In order to rationalize this surprising experimental finding, DFT total-energy calculations were performed. The QUANTUM ESPRESSO package [30] was used, employing the gradient-corrected PBE functional [31] for the description of the electron exchange and correlation. Relativistic effects are taken into account on different levels of theory: While for structure relaxation a scalar-relativistic description is found to be sufficient, spin-orbit coupling affects the details of the electronic structure considerably [5]. Hence, spectroscopic properties such as magnetic moments require multicomponent relativistic calculations [32,33] with noncollinear spin polarization. The latter is visualized by arrows in Figs. 2(b) and 2(c) for the calculated subsorption configurations I and II, respectively.

The Bi(111) surface is modeled by periodic supercells, which contain between 6 and 22 Bi bilayers [34] separated by 20 Å vacuum. The atoms in the bottom bilayer are kept fixed at their ideal bulk positions. All other atoms are freely relaxed. Numerically converged subsorption geometries are obtained using a $6 \times 6 \times 1$ Brillouin zone sampling and require 6 Bi(111) bilayer slabs with a (4×4) translational symmetry. Hence, the Bi(111) surface structure contains 193 Bi atoms, including the impurity. The incorporation energy profiles are investigated by keeping the z coordinate of the adatom fixed. Its lateral position, as well as the Bi atoms within the three uppermost bilayers are freely relaxed. Migration barriers are calculated by explicitly determining the corresponding saddle points via the nudged elastic band (NEB) approach [35].

IV. RESULTS AND DISCUSSION

The resulting reaction paths are shown in Fig. 2(a). In principle, the adatoms could adsorb at the surface (i) singly coordinated on top of a Bi atom of the first Bi layer or (ii) in two different threefold coordinated positions. However, for all investigated TM atoms a subsorbate position within the first Bi bilayer is the most stable configuration [labeled I in Fig. 2(a)]. Here, similar to the $CoSi_2$/Si(111) interface [36], the TM atoms are sevenfold coordinated: Six bonds are formed to the ligands within the first Bi bilayer. A seventh Bi atom from the second bilayer binds to the TM atom.

Interestingly, for the 3*d* transition metals the subsorbate incorporation in the first Bi bilayer turns out to be barrier free; i.e., no thermal activation is required. Only Sc shows a very weak, metastable minimum 0.48 Å above the surface separated by a very shallow barrier $\Delta E < 0.01$ eV from the stable subsorbate configuration. The interstitial configuration I is by far (∼1.1 eV) more stable than any substitutional incorporation, but energetically nearly degenerate with the fivefold coordinated interlayer position II [cf. Fig. 2(a)] as well as further intralayer positions deeper below the surface. However, migration into subsurface sites beyond configuration II is hindered by energy barriers of about 0.7 eV (Co) to 0.9 eV (Fe). The lateral mobility is restricted as well, but remains more probable: A lateral movement via configuration II and back into the top bilayer [cf. arrow in Fig. 2(a)] requires activation energies below 0.5 eV, and should thus occur prior to in-diffusion into the bulk.

The computational finding that the 3*d* TMs are captured at specific high-symmetry, sevenfold coordinated positions within the uppermost Bi bilayer is further corroborated by the comparison of the measured STM images with simulations based on the Tersoff-Hamann approach [37]: Only for the high-symmetry configuration I we obtain agreement with the measured STM data [cf. Fig. 1(d_1) and Fig. 2 showing Co as an example]. The three pronounced spots arise from $p-$like

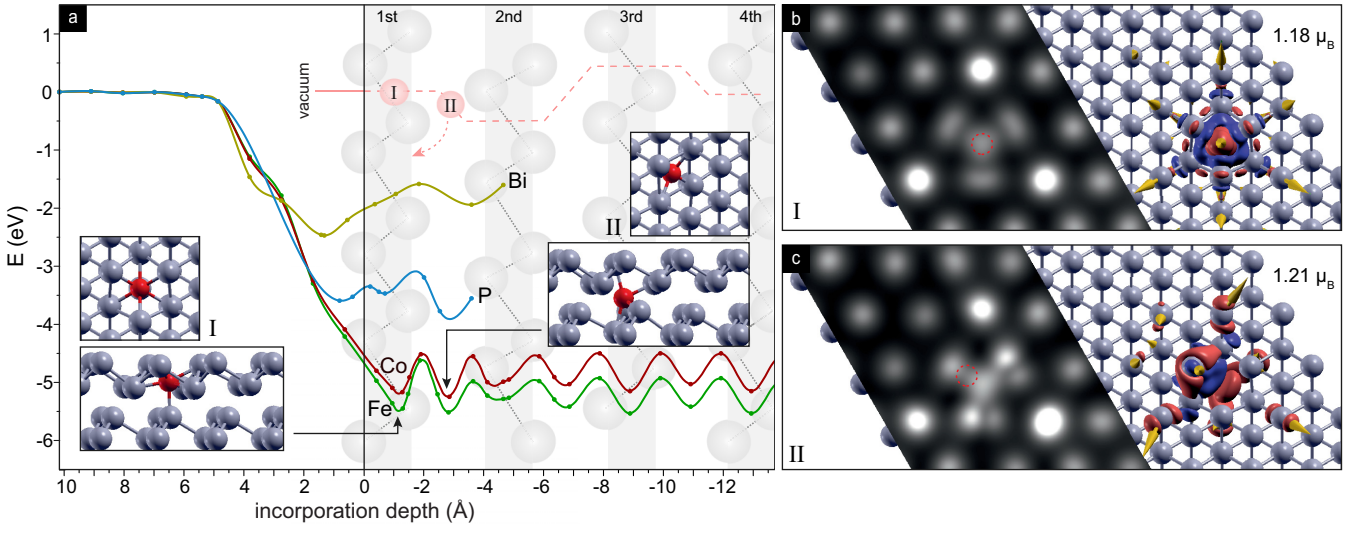

FIG. 2. (Color online) (a) Total energy for various adatom positions and different atomic species (Fe, Co, P, and Bi), the microscopic structures of the first (I) and second minimum (II), and the schematic migration path for a 3*d* TM atom (here Co) into the Bi bulk (arrow: relaxation in interlayer position as requirement for lateral motion). (b,c) Calculated STM image (constant current mode; $U = 10$ mV) for a single Co impurity in the highly symmetric sevenfold coordinated minimum I in the first bilayer and for the fivefold coordinated minimum II between two Bi bilayers. The red dashed circles indicate the position of the impurity Co atom. Co assumes a ferromagnetic configuration in both minima. The magnetization density induced by Co in minimum I and II (magnetic moments 1.18 and 1.21 μ_B, respectively) as well as the noncollinear spin orientation are indicated.

TABLE I. Calculated adsorption and incorporation energies (exothermic, in eV, relative to the respective free atom, metastable minima in brackets) calculated for various third, fourth, and fifth row element adatoms at or into the Bi(111) surface. If existing, energy barriers ΔE for the incorporation into the first Bi layer are also given.

	Sc	Ti	V	Cr	Mn	Fe	Co	Ni	Cu	Zn
Top	(3.53)	–	–	–	–	–	–	–	–	0.49
First BL	4.24	5.34	5.92	6.10	5.86	5.48	5.20	4.80	4.01	(0.26)
ΔE	<0.01	–	–	–	–	–	–	–	–	0.27
								Pd	Ag	
Top								(2.81)	(1.71)	
First BL								3.80	1.91	
ΔE								0.05	0.10	
	Bi	Pb						Pt	Au	
Top	2.60	2.61						(0.46)	(2.13)	
First BL	(1.58)	(1.75)						1.54	2.34	
ΔE	0.89	0.24						0.15	0.17	

orbitals at the next-nearest neighbor Bi surface atoms. The outer features of the experimental STM pattern cannot be reproduced within the 298 $Å^2$ surface of the (4×4) supercells, indicating that these features are resulting from delocalized 2D host states perturbed by the TM atom. Further information on the modification of the surface charge upon subsorption of TMs can be obtained from the calculated magnetization density shown in Fig. 2(b). For Co a magnetic moment of about $1.2\,\mu_B$ is calculated for both configurations, I as well as II. But the asymmetric charge distribution around the fivefold coordinated position II [cf. Fig. 2(c)] is not compatible with experiment: All measured STM images show scattering patterns with trigonal symmetry, indicative for configuration I. The impurities have apparently no transient mobility into the bulk. The energy gained from surface bonding is lost in dissipative processes during adsorption and subsorption, and the $3d$ TM atoms are trapped within the uppermost Bi bilayer. Thereby, the Fermi level is lifted by less than 10 meV with respect to the host states. It is their interstitial incorporation that allows the $3d$ TM impurity atoms to interact magnetically with the Rashba-split surface states (cf. Fig. 2) while only weakly perturbing the band structure.

In order to understand the special role of the $3d$ TMs, i.e., why they penetrate barrier-free, it is instructive to analyze the modification of their electronic configuration upon incorporation. The small shoulder in the energy profiles at about 3 Å above the first Bi bilayer [see Fig. 2(a)] is related to the onset of an electronic reconfiguration: The $3d$ TM atoms change their $3d^n 4s^2$ electronic configuration due to the interaction with the host material; i.e., the $4s$ levels are energetically lifted and donate charge into the d orbitals, a phenomenon well known for $3d$ TM point defects in bulk semiconductors [38,39] which allows the formation of highly coordinated σ bonds to neighboring atoms [40]. In the case of Co ($[Ar]3d^7\,4s^2$) approaching the Bi(111) film, for example, we find the occupation of the $4s$ states to be reduced to 0.64 and 0.47 electrons, 3 Å above and incorporated into the surface, respectively.

Looking at the process of incorporation in detail, the $3d$ TM atom first relaxes into the uppermost Bi layer and forms a planar configuration with three Bi ligands. Concurrently, the $3d$ electrons are polarized by the second layer Bi atoms and the impurity atom relaxes further without barrier towards the preferred, highly coordinated subsorbate position I within the Bi bilayer (see Fig. 2). The Bi lattice itself experiences only minor strain upon incorporation: The Bi-Bi bonds around the subsorbate change their length by amounts ranging from 2% (for Sc) up to at most 6% (for Cr). This is mainly related to a downwards relaxation of the second layer Bi atoms around the impurity. The topmost Bi atoms move laterally *towards* the impurity, but do essentially not vary their height; see inset I of Fig. 2. This agrees with the experimental observation that the topography of the surface remains unchanged.

$4d/5d$ TMs such as Pd and Pt also have partially filled d shells, but tend to form longer bonds with Bi. While their incorporation in the first Bi bilayer is still favorable, they have to overcome energy barriers ΔE of up to 0.2 eV (see Table I). This also holds for the noble metals Ag and Au. Atoms without partially filled d shell such as Zn, Bi, or Pb and even rather small atoms such as P and H cannot take advantage of the highly coordinated bonding position within the Bi bilayer. This position is either metastable or unstable for these atoms [cf. P and Bi in Fig. 2(a)] and they adsorb atop the surface.

That the barrier-free incorporation is actually a bond-length sensitive effect can also be seen by modifying the lateral lattice constant. This is of particular relevance for strained Bi(111) bilayer islands and substrate-stabilized Bi bilayers [22,23,19,24–26]. To obtain first estimates of how the atomic penetration will be influenced by strain, we perform additional total-energy calculations using single Bi(111) bilayers as a model systems. Thereby a barrier-free $3d$ TM incorporation into the bilayer is predicted, provided they are not too strongly strained. In case of Co deposition, for example, barrier-free incorporation occurs for bilayer strain between -5% and $+8\%$. For larger compression the lateral distance between neighboring Bi atoms and for more tensile strain above $+8\%$ the distance between the two Bi layers becomes too small. Therefore, we expect also systems that contain single, substrate-stabilized Bi(111) bilayers to be susceptible to the barrier-free incorporation, provided the lattice constant of the substrate is close to that of the Bi(111) surface. Hexagonal BN (-2%) or Bi_2Te_3 (-5%), e.g., fulfill this requirement. For

Bi_2Se_3, however, causing 11% compressive strain, thermal activation is required for a subsurface in-diffusion into the Bi bilayer.

V. SUMMARY

In this work, it has been demonstrated that the Bi(111) surface provides a specific incorporation site within the first bilayer, which is attractive for highly coordinated transition and noble metal atoms. They are found to penetrate the surface in a well defined way, thereby causing no morphological changes at the surface. In contrast to thermally activated in-diffusion recently found for Bi_2Se_3 and Bi_2Te_3 compound films [18,20,21], the incorporation of 3*d* TM into Bi(111) films occurs barrier-free. No annealing step is required reducing the probability for lateral migration and unwanted aggregation of the TM atoms in clusters to a minimum. Hence, high doping concentration become possible, and each atom assumes a well-defined sevenfold coordinated interstitial position, providing a metallic near-surface state by only weakly perturbing the band structure. The observed surface modification by barrier-free subsorption does not only allow for tuning the electronic properties of the Bi surfaces itself, but may also be applicable to topological insulators formed by substrate-stabilized Bi bilayers, provided the lattice constant of the substrate resembles within a few percent that of the Bi(111) surface; otherwise in-diffusion requires thermal activation.

ACKNOWLEDGMENTS

We acknowledge financial support by the DFG through SFB 616, SPP 1601, and Pf238/31 as well as grants of high-performance computer time from the HLRS Stuttgart and the Paderborn PC^2. Research was carried out in part at the Center for Functional Nanomaterials, Brookhaven National Laboratory, which is supported by the U.S. Department of Energy, Office of Basic Energy Sciences, under Contract No. DE-AC02-98CH10886.

[1] C. R. Ast, J. Henk, A. Ernst, L. Moreschini, M. C. Falub, D. Pacile, P. Bruno, K. Kern, and M. Grioni, Phys. Rev. Lett. **98**, 186807 (2007).
[2] Ph. Hofmann, Prog. Surf. Sci. **81**, 191 (2006).
[3] T. Hirahara, T. Nagao, I. Matsuda, G. Bihlmayer, E. V. Chulkov, Yu. M. Koroteev, P. M. Echenique, M. Saito, and S. Hasegawa, Phys. Rev. Lett. **97**, 146803 (2006).
[4] E. I. Rashba, Sov. Phys. Solid State **2**, 1109 (1960).
[5] Yu. M. Koroteev, G. Bihlmayer, J. E. Gayone, E. V. Chulkov, S. Blügel, P. M. Echenique, and Ph. Hofmann, Phys. Rev. Lett. **93**, 046403 (2004).
[6] T. Hirahara, K. Miyamoto, I. Matsuda, T. Kadono, A. Kimura, T. Nagao, G. Bihlmayer, E. V. Chulkov, S. Qiao, K. Shimada, H. Namatame, M. Taniguchi, and S. Hasegawa, Phys. Rev. B **76**, 153305 (2007).
[7] M. C. Cottin, C. A. Bobisch, J. Schaffert, G. Jnawali, A. Sonntag, G. Bihlmayer, and R. Möller, Appl. Phys. Lett. **98**, 022108 (2011).
[8] G. Jnawali, C. Klein, Th. Wagner, H. Hattab, P. Zahl, D. P. Acharya, P. Sutter, A. Lorke, and M. Horn-von Hoegen, Phys. Rev. Lett. **108**, 266804 (2012).
[9] Z. Wang, T. Lin, P. Wei, X. Liu, R. Dumas, K. Liu, and J. Shi, Appl. Phys. Lett. **97**, 042112 (2010).
[10] D. Hsieh, Y. Xia, L. Wray, D. Qian, A. Pal, J. H. Dil, J. Osterwalder, F. Meier, G. Bihlmayer, C. L. Kane, Y. S. Hor, R. J. Cava, and M. Z. Hasan, Science **323**, 919 (2009).
[11] T. Hirahara, N. Fukui, T. Shirasawa, M. Yamada, M. Aitani, H. Miyazaki, M. Matsunami, S. Kimura, T. Takahashi, S. Hasegawa, and K. Kobayashi, Phys. Rev. Lett. **109**, 227401 (2012).
[12] D. Lükermann, S. Sologub, H. Pfnür, C. Klein, M. Horn-von Hoegen, and C. Tegenkamp, Phys. Rev. B **86**, 195432 (2012).
[13] Z. Alpichshev, R. R. Biswas, A. V. Balatsky, J. G. Analytis, J.-H. Chu, I. R. Fisher, and A. Kapitulnik, Phys. Rev. Lett. **108**, 206402 (2012).
[14] G. Wang, X.-G. Zhu, Y.-Y. Sun, Y.-Y. Li, T. Zhang, J. Wen, X. Chen, K. He, L.-L. Wang, X.-C. Ma, J.-F. Jia, S. B. Zhang, and Q.-K. Xue, Adv. Mater. **23**, 2929 (2011).
[15] C. Mann, D. West, I. Miotowski, Y. P. Cheng, S. Zhang, and C.-K. Shih, Nat. Commun. **4**, 2277 (2013).
[16] T. Zhang, P. Cheng, X. Chen, J.-F. Jia, X. Ma, K. He, L. Wang, H. Zhang, X. Dai, Z. Fang, X. Xie, and Q.-K. Xue, Phys. Rev. Lett. **103**, 266803 (2009)
[17] J. Seo, P. Roushan, H. Beidenkopf, Y.-S. Hor, R.-J. Cava, and A. Yazdani, Nature **466**, 343 (2010).
[18] T. Schlenk, M. Bianchi, M. Koleini, A. Eich, O. Pietzsch, T. O. Wehling, T. Frauenheim, A. Balatsky, J.-L. Mi, B. B. Iversen, J. Wiebe, A. A. Khajetoorians, Ph. Hofmann, and R. Wiesendanger, Phys. Rev. Lett. **110**, 126804 (2013).
[19] M. Cottin, C. A. Bobisch, J. Schaffert, G. Jnawali, G. Bihlmayer, and R. Möller, Nano Lett. **13**, 2717 (2013).
[20] D. West, Y. Y. Sun, S. B. Zhang, T. Zhang, X. Ma, P. Cheng, Y. Y. Zhang, X. Chen, J. F. Jia, and Q. K. Xue, Phys. Rev. B **85**, 081305(R) (2012).
[21] C. L. Song, Y. P. Jiang, Y. L. Wang, Z. Li, L. Wang, K. He, X. Chen, X. C. Ma, and Q. K. Xue, Phys. Rev. B **86**, 045441 (2012).
[22] T. Hirahara, G. Bihlmayer, Y. Sakamoto, M. Yamada, H. Miyazaki, S. Kimura, S. Blügel, and S. Hasegawa, Phys. Rev. Lett. **107**, 166801 (2011).
[23] M. Chen, J.-P. Peng, H.-M. Zhang, L-L Wang, K. He, X.-C. Ma, and Q.-K. Xue, Appl. Phys. Lett. **101**, 081603 (2012).
[24] S. H. Kim, K.-H. Jin, J. Park, J. S. Kim, S.-H. Jhi, T.-H. Kim, and H. W. Yeom, Phys. Rev. B **89**, 155436 (2014).
[25] A. Eich, M. Michiardi, G. Bihlmayer, X.-G. Zhu, J.-L. Mi, B. B. Iversen, R. Wiesendanger, Ph. Hofmann, A. A. Khajetoorians, and J. Wiebe, Phys. Rev. B **90**, 155414 (2014).
[26] I. K. Drozdov, A. Alexandradinata, S. Jeon, S. Nadj-Perge, H. Ji, R. J. Cava, B. A. Bernevig, and A. Yazdani, Nat. Phys. **10**, 664 (2014).
[27] T. Payer, C. Klein, M. Acet, V. Ney, M. Kammler, F.-J. Meyer zu Heringdorf, and M. Horn-von Hoegen, Thin Solid Films **520**, 6905 (2012).
[28] G. Jnawali, Th. Wagner, H. Hattab, R. Möller, A. Lorke, and M. Horn-von Hoegen, e-J. Surf. Sci. Nanotechnol. **8**, 27 (2010).

[29] T. Hirahara, I. Matsuda, S. Yamazaki, N. Miyata, S. Hasegawa, and T. Nagao, Appl. Phys. Lett. **91**, 202106 (2007).
[30] P. Giannozzi *et al.*, J. Phys.: Condens. Matter **21**, 395502 (2009); http://www.quantum-espresso.org.
[31] J. P. Perdew, K. Burke, and M. Ernzerhof, Phys. Rev. Lett. **77**, 3865 (1996).
[32] A. DalCorso, Phys. Rev. B **82**, 075116 (2010).
[33] U. Gerstmann, N. J. Vollmers, A. Lücke, M. Babilon, and W. G. Schmidt, Phys. Rev. B **89**, 165431 (2014).
[34] Y. M. Koroteev, G. Bihlmayer, E. V. Chulkov, and S. Blügel, Phys. Rev. B **77**, 045428 (2008).
[35] G. Henkelmann and H. Jónsson, J. Chem. Phys. **113**, 9978 (2000).
[36] M. F. Chisholm, S. J. Pennycock, R. Jebasinski, and S. Mantl, Appl. Phys. Lett. **64**, 2409 (1994).
[37] J. Tersoff and D. Hamann, Phys. Rev. B **31**, 805 (1985).
[38] F. Beeler, O. K. Andersen, and M. Scheffler, Phys. Rev. Lett. **55**, 1498 (1985).
[39] U. Gerstmann, A. T. Blumenau, and H. Overhof, Phys. Rev. B **63**, 075204 (2001).
[40] A. Abragam and B. Bleeney, *Electron Paramagnetic Resonance of Transition Ions* (Dover Publications, New York, 1989).